Letter

Magneto-optical measurements of the negatively charged 2*s* exciton in WSe₂

J. C. Sell [1,*] J. R. Vannucci [1,*] D. G. Suárez-Forero [1] B. Cao,[1] D. W. Session,[1] H.-J. Chuang [2,†] K. M. McCreary [3] M. R. Rosenberger [4] B. T. Jonker [3] S. Mittal,[5] and M. Hafezi [1,6]

[1]*Joint Quantum Institute, NIST and University of Maryland, College Park, Maryland 20742, USA*
[2]*Nova Research, Incorporated, Washington, DC 20375, USA*
[3]*Naval Research Laboratory, Washington, DC 20375, USA*
[4]*Department of Aerospace and Mechanical Engineering, University of Notre Dame, Notre Dame, Indiana 46556, USA*
[5]*Department of Electrical and Computer Engineering, Northeastern University, Boston, Massachusetts 02115, USA*
[6]*Department of Electrical Engineering and Institute for Research in Electronics and Applied Physics,
University of Maryland, College Park, Maryland 20742, USA*

Monolayer transition metal dichalcogenides (TMDs) host a variety of optically excited quasiparticle species that stem from two-dimensional confinement combined with relatively large carrier effective masses and reduced dielectric screening. The magnetic response of these quasiparticles gives information on their spin and valley configurations, nuanced carrier interactions, and insight into the underlying band structure. Recently, there have been several reports of $2s/3s$ charged excitons in TMDs, but very little is still known about their response to external magnetic fields. Using photoluminescence excitation spectroscopy, we observe the presence of the $2s$ charged exciton and report its response to an applied magnetic field. We benchmark this response against the neutral exciton and find that both the $2s$ neutral and charged excitons exhibit similar behavior with g factors of $g_{X_0^{2s}} = -5.20 \pm 0.11$ and $g_{X_-^{2s}} = -4.98 \pm 0.11$, respectively.

Monolayer semiconductor transition metal dichalcogenides (TMDs) have attracted significant attention in the last decade due to their unique optical properties. Similar to graphene, but with a three-layer (staggered) honeycomb lattice, TMDs host direct-gap transitions at their $\pm K$ valleys and exhibit circular dichroism due to their finite Berry curvature [1–3]. The reduced dimensionality of materials in this system, coupled with techniques such as hexagonal boron nitride (hBN) encapsulation, lead to an enhanced Coulomb interaction and excitons with large binding energies ($E_B \approx$ 150–500 meV) [4–6].

When there is excess charge present in the system during exciton formation, the exciton may lower its energy by capturing an electron or hole and form a bound, charged three-body state referred to as a charged exciton. Charged excitons are a ubiquitous feature of semiconductors, but are difficult to observe in traditional systems—such as GaAs/AlGaAs quantum wells—due to their small binding energies (1–2 meV) [9–11]. In TMDs, however, both singlet and triplet charged species have been discovered with $E_B \approx$ 20–40 meV [8,12–15]. In the high carrier density regime, these resonances have been alternatively interpreted as many-body polaron states [16–19].

In analogy to the hydrogen atom, excitons are known to form a Rydberg series of higher-energy states [20]. In TMDs,

they have been observed through a variety of different optical techniques up to principal quantum number $n = 11$ [4,5,21–24]. However, even in the presence of excess charge, a corresponding series for the charged exciton has remained elusive. The lack of experimental observations of these states has been thought of analogously to the H⁻ ion, for which there exists no bound excited state [25]. More recent theoretical work [26–29] has detailed scenarios in which these higher n charged excitons could exist, but that work does not match with a series of compelling experimental reports of metastable $2s/3s$ charged excitons in TMDs [30–33]. Significant work remains to reconcile experimental results with theoretical understanding.

The difficulty in observing these higher n states is twofold: (I) The weak radiative decay rate of excitons with higher n makes them increasingly dim in typical photoluminescence (PL) measurements [34] and (II) even once the state is observed optically, further carrier density and magnetic-field-dependent measurements are needed to correctly identify the exciton species. In particular, the magneto-optical characterization of exciton species has proven to be an important tool for distinguishing between particle configurations [35,36]. It also gives valuable information about the spin-valley character of each excitation [13,14,37–39], many-body interaction [16,40,41], and the underlying band structure of the materials themselves [42–46].

In this Letter, we confirm the presence of negatively charged $2s$ exciton (X_-^{2s}) in WSe₂ via photoluminescence excitation (PLE) measurements. In PLE, we monitor the emission from the $1s$ (lowest-energy) exciton species while the

─────────
*These authors contributed equally to this work.
†Present address: Naval Research Laboratory, Washington, DC 20375, USA.
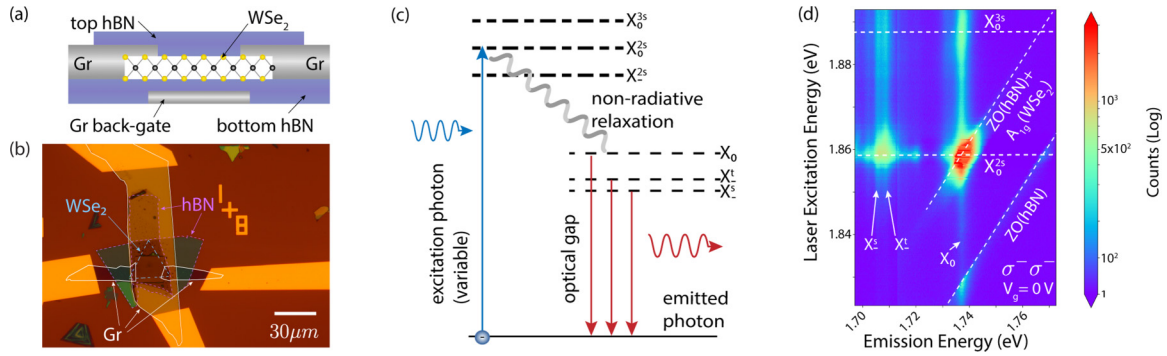
FIG. 1. (a) Schematic of the hBN encapsulated WSe_2 with a graphite (Gr) back gate and electrodes. (b) Optical image of device after full fabrication. The compressed area in the center indicates the region of the sample that underwent nanosqueegeeing. (c) Schematic of the PLE process highlighting the higher n states (e.g., X_0^{2s}) and emission monitored channels (e.g., X_0, X_-^t, or X_-^s). (d) $\sigma^-\sigma^-$ PLE spectra taken at $V_g = 0$ V and sample temperature of <300 mK. The monitored emission channels are marked with arrows (X_0, X_-^t, and X_-^s) [47,48]. Two Raman modes are identified as diagonal dashed lines [ZO(hBN) and ZO(hBN) $+ A_{1g}(WSe_2)$] (see Refs. [49–51]). The resonances of the excited states are marked with horizontal dashed lines (X_0^{2s}, X_0^{3s}) [22].

excitation laser's energy was swept in the energy regime needed to resonantly probe higher n states. This provides a superior signal-to-noise ratio compared to PL. Additionally, we report on the response of X^{2s} to an applied magnetic field. We measure the valley-dependent Zeeman splitting for both the 2s neutral (X_0^{2s}) and charged (X_-^{2s}) excitons in the carrier density regime in which they coexist. From this, we extract similar g factors for X_0^{2s}/X_-^{2s}, $g_{X_0^{2s}} = -5.20 \pm 0.11$ and $g_{X_-^{2s}} = -4.98 \pm 0.11$, and discuss the possible physical origins of this result.

In our experiment, a monolayer of chemical vapor deposition (CVD) grown WSe_2 is encapsulated in hBN along with few-layer graphite (Gr) contacts and a bottom gate electrode. Encapsulation was performed via the wet capillary action method and interlayer contamination was removed via the nanosqueegee method [52] [see Fig. 1(a) for a schematic of the sample and Fig. 1(b) for an image of the final device]. The full fabrication details are reported in the Supplemental Material (SM [49], which includes Refs. [53–70]). The joint hBN and Gr encapsulation allows for a high-quality device with electrostatic control over the carriers in the system via the applied gate voltage V_g [71].

Throughout our work, we utilize PLE to resonantly probe the 2s exciton states. In PLE, the energy of the input photons is varied and when their energy resonantly matches a 2s exciton state, electrons are excited from the valence band to form these excitons (e.g., X_0^{2s}). There, the 2s excitons undergo nonradiative relaxation to a 1s state (e.g., the neutral exciton X_0) where they radiatively recombine and emit photons. An illustration of this process is shown in Fig. 1(c). For these measurements, the excitation beam is generated using a dye laser with a dynamic excitation range of 1.77–1.99 eV. We use a confocal configuration with circular polarization resolution in both excitation and detection. Throughout this Letter, we denote the excitation/emission polarization in the format $\sigma^{excitation}\sigma^{emission}$. The sample was placed in a dilution refrigerator equipped with a 12-T superconducting magnet in a Faraday geometry. We estimate that with residual heating from the laser and magnet, the ambient temperature of the sample is <300 mK.

Figure 1(d) shows a baseline PLE spectrum taken with $\sigma^-\sigma^-$ ($-K$-valley selective) at $V_g = 0$ V and $B = 0$ T. We identify the 2s and 3s neutral Rydberg excitons (X_0^{2s}, X_0^{3s}) by their binding energies [24,72] and labeled them with white dashed lines at 1.859 and 1.887 eV, respectively. The 1s neutral (X_0) exciton's emission channel and the triplet (X_-^t)/singlet (X_-^s) charged excitons' emission channels were identified by their binding energies [48,73] and PL gate voltage dependence [74] (see SM [49]).

Next, we tune V_g to n_e-dope the system and look for signs of an emerging charged 2s exciton in our PLE spectra. Figure 2 highlights the results of this while monitoring the X_0 emission channel; Fig. 2(a) shows the full PLE spectra at selected V_g, while Fig. 2(b) is the integrated vertical cross section of the emission spectrum around the X_0 signal. The integration region used for all gate voltages is denoted in the $V_g = 0.6$ V panel of Fig. 2(a) by the vertical dashed lines. As in Fig. 1, we identify the resonance at 1.859 eV as X_0^{2s}.

At $V_g = 0.3$ V, a lower-energy resonance begins to emerge at 1.838 eV. We label this state as the 2s charged exciton X_-^{2s} and base this identification on two observations: (I) $V_g = 0.3$ V corresponds to the transition of the sample from charge neutrality to n_e doped and the emergence of the negatively charged 1s excitons X_-^t/X_-^s (see SM [49] for 1s PL data). The X_-^{2s} resonance displays a similar onset at $V_g = 0.3$ V indicating a similar negative charge character. (II) When the X_-^{2s} resonance first appears at $V_g = 0.3$ V, we find that $\Delta E_{(X_0^{2s}-X_-^{2s})} = 21$ meV while $\Delta E_{(X_0-X_-^t)} = 29$ meV and $\Delta E_{(X_0-X_-^s)} = 35$ meV. This reduction indicates that the 2s charged exciton is less tightly bound than its 1s state counterpart. This is in accordance with other observations in the literature [30–33] and consistent with the fact that Rydberg states display a reduction in relative binding energy with each increasing n.

Since the 2s charged exciton is expected to be a doublet, as observed for the 1s charged excitons, the extracted position of X_-^{2s} is an average. X_-^t and X_-^s have a narrow linewidth and a strong intervalley exchange interaction that splits them (≈ 6 meV [15,75]) which allows us to spectrally resolve them. However, the broadness of the 2s states combined with a
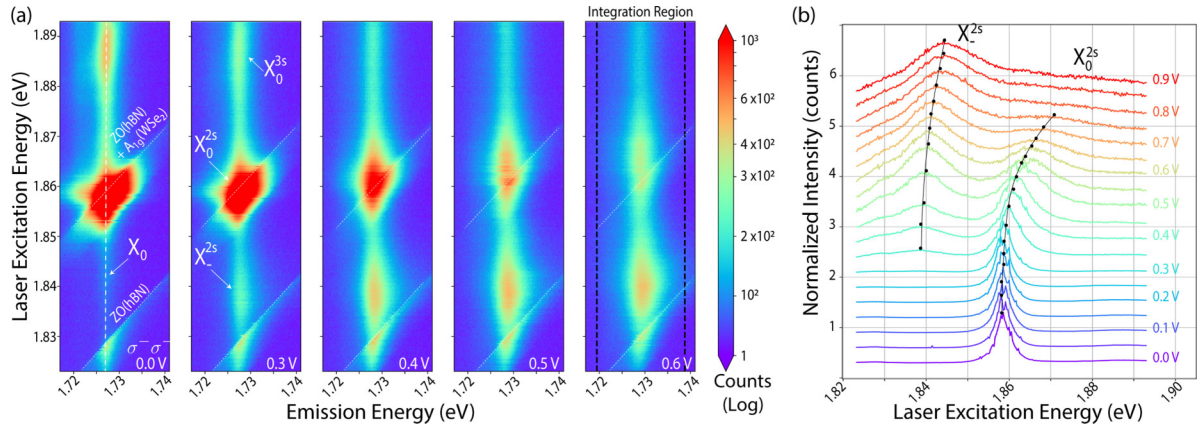
FIG. 2. (a) PLE data with increasing n_e doping while monitoring the X_0 recombination channel in the $-K$ valley ($\sigma^-\sigma^-$). (b) Waterfall plot of vertical cross sections from $V_g = 0$ to 0.9 V. The integration region is annotated in (a). The counts were summed over the emission width for each excitation energy.

reduced intervalley exchange energy (theoretically predicted to be ≈ 1 meV [32,75]) prevents us from resolving the doublet of the 2s charged exciton. There is, however, indication of the two states in the asymmetric line shape of the X_-^{2s} peak (see SM [49]).

In Fig. 2(b), we see the spectral dependence of X_0^{2s} and X_-^{2s} with carrier density. As the n_e doping increases with increasing gate voltage, the X_0^{2s} resonance broadens, decreases in intensity, and spectrally blueshifts. The broadening and loss of spectral intensity are consistent with more rapid decoherence from an interaction with the Fermi sea. The blueshift results from the competing effects of the band gap and binding energy renormalization due to decreased $e^- \text{-} e^-$ and $e^- \text{-} h^+$ interaction from screening by the Fermi sea [33,76,77].

In contrast, the X_-^{2s} peak grows in intensity and experiences minimal spectral drift with increased carrier density. In the case of a three-body quasiparticle, one expects a redshift that is linearly dependent on the charge concentration in the system resulting from momentum conservation [12,19,76]. This competes with the effects of band gap and binding energy renormalization previously discussed for the neutral excitons that favor a blueshift [76], and leads to the minimal spectral

drift observed. Both the increase in intensity and small spectral shift are consistent with the behavior of 1s and 2s charged excitons previously observed [33,76,77].

Since X_-^{2s} emerges in the n_e-doped regime, we expect X_-^t and X_-^s to be the most prominent emission channels for 2s exciton species (see SM [49]). To verify this, we monitor the X_-^t emission channel in a similar manner to X_0 and show the results as a function of V_g in Fig. 3 (the results for X_-^s can be found in SM [49]). We confirm that the behavior (spectral position, shift with gate, etc.) of X_0^{2s} and X_-^{2s} is independent of the monitored decay channel.

We turn our attention to extracting the behavior of the X_0^{2s} and X_-^{2s} with applied magnetic field. We chose to take the data at $V_g = 0.6$ V because both the neutral and charged exciton have a similar intensity. Integrated vertical cross sections of the X_-^t emission channel presented in Figs. 4(a) and 4(b) show the response of the $-K(\sigma^-\sigma^-)$ and $+K(\sigma^+\sigma^+)$ valleys, respectively, with magnetic field. The extracted peak centers from fitting are marked with black dots. Applying a magnetic field breaks the time-reversal symmetry in the system, and results in a redshift (blueshift) with positive field for the $+K$ $(-K)$ valley and vice versa with applied negative field [13,16].
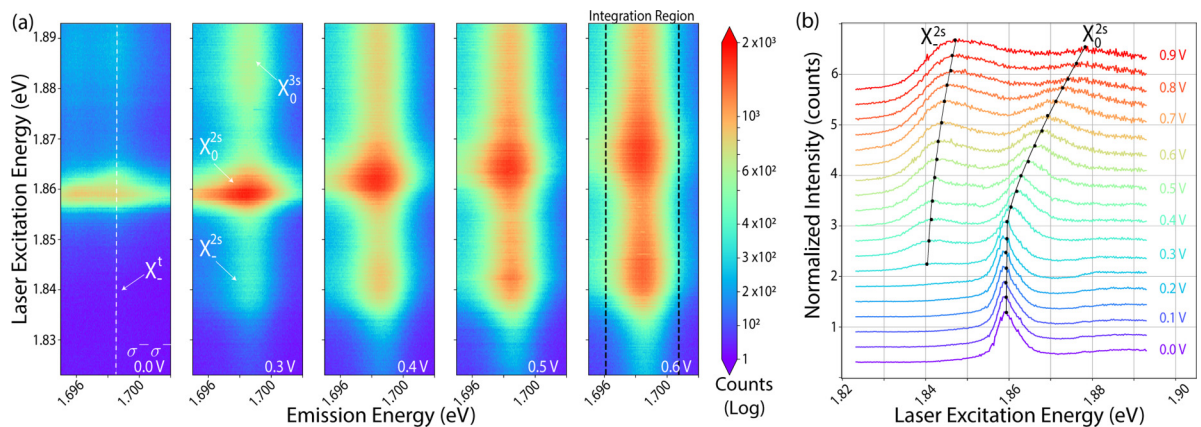

FIG. 3. (a) PLE data with increasing n_e doping while monitoring the X_-^t recombination channel ($\sigma^-\sigma^-$). (b) As in Fig. 2, the waterfall plot corresponds to vertical cross sections from $V_g = 0$ to 0.9 V.
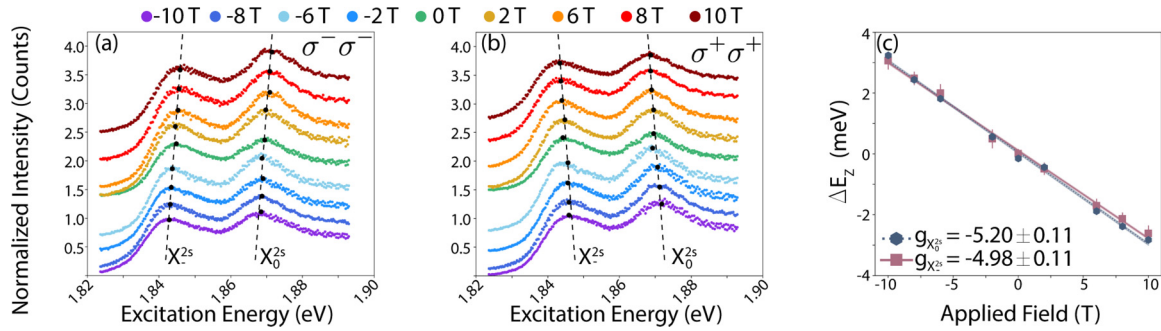
FIG. 4. Vertical cross sections from the X^t_- emission channel as a function of field for (a) $(\sigma^-\sigma^-)$ and (b) $(\sigma^+\sigma^+)$ marked with the corresponding peak positions (black dots) for the X^{2s}_0 and X^{2s}_- states from fitting with the dashed line serving as a guide to the eye. (c) Extracted g factors for X^{2s}_0 and X^{2s}_- states. The thickness of the fit line in (c) corresponds to the error in the fit.

Using the definition for the Zeeman splitting in terms of polarization components, $\Delta E_Z = E^{\sigma^+\sigma^+} - E^{\sigma^-\sigma^-} = g\mu_B B$, we fit a linear model to our data and extract a g factor of -5.20 ± 0.11 and -4.98 ± 0.11 for X^{2s}_0 and X^{2s}_-, respectively. This fit and extracted difference is shown in Fig. 4(c). Results that agreed within experimental error were found for both X^{2s}_0 and X^{2s}_- for a similar analysis of the X^s_- emission channel (see SM [49]).

Frequently, a single-particle model is used to interpret the g factor for $1s$ excitons. In this model, the contributions to the Zeeman splitting are defined as $\Delta E_Z = -\vec{\mu} \cdot \vec{B}$. The magnetic moment $\vec{\mu}$ is composed of additive terms for the orbital and spin contributions (intracellular components μ_O, μ_S) along with a correction for the effects of the finite Berry curvature in the system (intercellular component μ_V) [38,39,44,75,78] in each relevant band. Within this interpretation, we expect $g_{X_0} \approx -4.4$ and $-11 \lesssim g_{X^{t/s}_-} \lesssim -4$ (depending on the method used to calculate μ_V, and whether the doublet is resolved [13,14,47]).

To serve as a reference point between the literature and our $2s$ results, we also extracted the g factors for X_0 and $X^{t/s}_-$. These values are $g_{X_0} = -4.22 \pm 0.04$, $g_{X^t_-} = -4.12 \pm 0.04$, and $g_{X^s_-} = -3.86 \pm 0.05$ in our system at $V_g = 0.6$ V. They are consistent with the results from the single-particle interpretation, but highlight a distinct increase in our $2s$ g factors with respect to the corresponding $1s$ states. We discuss two possible contributions to this enhancement.

(I) Enhancement of the g factor for the $2s$ neutral exciton has been observed in magnetic Rydberg measurements in both intrinsic and electrostatically neutral samples [21,23,24]. Since the observation in neutral samples rules out doping effects, the divergence from $g_{X_0} \approx -4.4$ has been attributed to enhanced intercellular contributions arising from the increased k-space localization of the wave functions with each subsequent n [24]. Extending this technique to charged excitons gives an intercellular component that *decreases* as the Bohr radius *increases*. This is compounded by an increased k-space localization of the charged exciton (see SM [49]). While this model could explain the results for X^{2s}_0 it would underestimate the g factor for X^{2s}_-.

(II) A second possibility is the onset of a many-body interaction (polaron picture) between the excitons and the emerging Fermi sea from electrostatic gating. Many-body in-

teractions are expected to be very favorable in WSe$_2$ which has a Wigner-Seitz radius greater than 1 even at extremely high densities [41,79]. The interaction strength will vary with the Fermi sea's population and the Bohr radius, and induce Fermi sea polarization. A carrier-dependent enhancement of the g factor in TMDs has been documented for many materials/quasiparticles, with the strength of enhancement dictated by the degree of the induced Fermi sea polarization [16,37,40,41].

In the many-body picture, it has been observed that as doping levels are varied there is a convergence of the g factor between competing quasiparticles (e.g., X_0 and X^-) in regions in which they coexist. In analogy to the Kondo effect, the impurity (exciton) is dressed with either an attractive or repulsive interaction with the Fermi sea. As the carrier density increases, the state dressing will become more similar for all exciton species—regardless of the type of interaction—resulting in a convergence of the g factors [40] for X_0-like and X_--like excitons. Such behavior is not expected to be limited to the $1s$ state excitons and can explain the convergence of our extracted values of g for the X^{2s}_0 and X^{2s}_- within experimental error.

Our results serve as a marker in mapping the behavior of the $2s$ charged state X^{2s}_- with magnetic field in TMDs. Experimental quantification of the g factor serves as another physical benchmark for future theoretical models of stable $2s$ charged states. Additionally, the stability of the X^{2s}_- state offers a possible medium for studying the crossover from exciton Rydberg physics to the quantum Hall regime for charged species at high magnetic fields. Recent work by Klein *et al.* used carrier-density-dependent g-factor measurements to demonstrate tunable many-body physics through all $1s$ exciton species in MoS$_2$ [40]. Our initial results indicate that it would be possible to produce this type of map for $2s$ species with access to higher magnetic fields and devices with a larger dynamic carrier density range. This opens up a unique opportunity to study many-body interactions in higher-energy exciton species that is generally limited in traditional semiconductors systems with smaller exciton binding, such as GaAs quantum wells.

[1] K. Mak, K. McGill, J. Park, and P. McEuen, Science **344**, 1489 (2014).

[2] D. Xiao, G. B. Liu, W. Feng, X. Xu, and W. Yao, Phys. Rev. Lett. **108**, 196802 (2012).

[3] K. F. Mak, C. Lee, J. Hone, J. Shan, and T. F. Heinz, Phys. Rev. Lett. **105**, 136805 (2010).

[4] A. Stier, K. McCreary, B. Jonker, J. Kono, and S. Crooker, Nat. Commun. **7**, 10643 (2016).

[5] A. Chernikov, T. C. Berkelbach, H. M. Hill, A. Rigosi, Y. Li, B. Aslan, D. R. Reichman, M. S. Hybertsen, and T. F. Heinz, Phys. Rev. Lett. **113**, 076802 (2014).

[6] K. He, N. Kumar, L. Zhao, Z. Wang, K. F. Mak, H. Zhao, and J. Shan, Phys. Rev. Lett. **113**, 026803 (2014).

[7] M. Lampert, Phys. Rev. Lett. **1**, 450 (1958).

[8] J. Ross, S. Wu, H. Yu, N. Ghimire, A. Jones, G. Aivazian, J. Yan, D. Mandrus, D. Xiao, W. Yao, and X. Xu, Nat. Commun. **4**, 1474 (2013).

[9] K. Kheng, R. T. Cox, M. Y. d'Aubigné, F. Bassani, K. Saminadayar, and S. Tatarenko, Phys. Rev. Lett. **71**, 1752 (1993).

[10] G. Finkelstein, H. Shtrikman, and I. Bar-Joseph, Phys. Rev. B **53**, R1709 (1996).

[11] V. V. Solovyev and I. V. Kukushkin, Phys. Rev. B **79**, 233306 (2009).

[12] K. F. Mak, K. He, C. Lee, G. Lee, J. Hone, T. F. Heinz, and J. Shan, Nat. Mater. **12**, 207 (2013).

[13] A. Srivastava, M. Sidler, A. Allain, D. Lembke, A. Kis, and Imamoğlu, Nat. Phys. **11**, 141 (2015).

[14] T. Lyons, S. Dufferwiel, M. Brooks, F. Withers, T. Taniguchi, K. Watanabe, K. Novoselov, G. Burkard, and A. Tartakovskii, Nat. Commun. **10**, 2330 (2019).

[15] E. Courtade, M. Semina, M. Manca, M. M. Glazov, C. Robert, F. Cadiz, G. Wang, T. Taniguchi, K. Watanabe, M. Pierre, W. Escoffier, E. L. Ivchenko, P. Renucci, X. Marie, T. Amand, and B. Urbaszek, Phys. Rev. B **96**, 085302 (2017).

[16] P. Back, M. Sidler, O. Cotlet, A. Srivastava, N. Takemura, M. Kroner, and A. Imamoğlu, Phys. Rev. Lett. **118**, 237404 (2017).

[17] M. Sidler, P. Back, O. Cotlet, A. Srivastava, T. Fink, M. Kroner, E. Demler, and A. Imamoğlu, Nat. Phys. **13**, 255 (2017).

[18] M. M. Glazov, J. Chem. Phys. **153**, 034703 (2020).

[19] D. Efimkin and A. H. MacDonald, Phys. Rev. B **95**, 035417 (2017).

[20] T. Kazimierczuk, D. Frölich, S. Scheel, H. Stolz, and M. Bayer, Nature (London) **514**, 343 (2014).

[21] T. Wang, Z. Li, Y. Li, Z. Lu, S. Miao, Z. Lian, Y. Meng, M. Blei, T. Taniguchi, K. Watanabe, S. Tongay, D. Smirnov, C. Zhang, and S.-F. Shi, Nano Lett. **20**, 7635 (2020).

[22] A. V. Stier, N. P. Wilson, K. A. Velizhanin, J. Kono, X. Xu, and S. A. Crooker, Phys. Rev. Lett. **120**, 057405 (2018).

[23] M. Goryca, J. Li, A. V. Stier, T. Taniguchi, K. Watanabe, E. Courtade, S. Shree, C. Robert, B. Urbaszek, X. Marie, and S. A. Crooker, Nat. Commun. **10**, 4172 (2019).

[24] S.-Y. Chen, Z. Lu, T. Goldstein, J. Tong, A. Chaves, J. Kunstmann, T. Cavalcante, L.S.R. in Woźniak, G. Seifert,

D. R. Reichman, T. Taniguchi, K. Watanabe, D. Smirnov, and J. Yan, Nano Lett. **19**, 2464 (2019).

[25] R. N. Hill, Phys. Rev. Lett. **38**, 643 (1977).

[26] C. Fey, P. Schmelcher, A. Imamoğlu, and R. Schmidt, Phys. Rev. B **101**, 195417 (2020).

[27] J. Yan and K. Varga, Phys. Rev. B **101**, 235435 (2020).

[28] A. Rau, J. Astrophys. Astron. **17**, 113 (1996).

[29] S. Y. Shiau, M. Combescot, and Y.-C. Chang, Phys. Rev. B **86**, 115210 (2012).

[30] T. Goldstein, Y.-C. Wu, S.-Y. Chen, T. Taniguchi, K. Watanabe, K. Varga, and J. Yan, J. Chem. Phys. **153**, 071101 (2020).

[31] E. Liu, J. van Baren, Z. Lu, T. Taniguchi, K. Watanabe, D. Smirnov, Y.-C. Chang, and C. Lui, Nat. Commun. **12**, 6131 (2021).

[32] A. Arora, T. Deilmann, T. Reichenauer, J. Kern, S. Michaelis de Vasconcellos, M. Rohlfing, and R. Bratschitsch, Phys. Rev. Lett. **123**, 167401 (2019).

[33] K. Wagner, E. Wietek, J. D. Ziegler, M. A. Semina, T. Taniguchi, K. Watanabe, J. Zipfel, M. M. Glazov, and A. Chernikov, Phys. Rev. Lett. **125**, 267401 (2020).

[34] H. Haug and S. W. Koch, *Quantum Theory of the Optical and Electronic Properties of Semiconductors*, 4th ed. (World Scientific, Singapore, 2004).

[35] E. Liu, J. van Baren, T. Taniguchi, K. watanabe, Y.-C. Chang, and C. H. Lui, Phys. Rev. Research **1**, 032007(R) (2019).

[36] M. He, P. Rivera, D. Van Tuan, N. P. Wilson, M. Yang, T. Taniguchi, K. Watanabe, J. Yan, D. Mandrus, H. Yu, H. Dery, W. Yao, and X. Xu, Nat. Commun. **11**, 618 (2020).

[37] Z. Li, T. Wang, C. Jin, Z. Lu, Z. Lian, Y. Meng, M. Blei, S. Gao, T. Taniguchi, K. Watanabe, T. Ren, S. Tongay, L. Yang, D. Smirnov, T. Cao, and S.-F. Shi, Nat. Commun. **10**, 2469 (2019).

[38] D. MacNeill, C. Keikes, K. F. Mak, Z. Anderson, A. Kormányos, V. Zólyomi, J. Park, and D. Ralph, Phys. Rev. Lett. **114**, 037401 (2015).

[39] Y. Li, J. Ludwig, T. Low, A. Chernkiov, X. Cui, G. Arefe, Y. D. Kim, A. M. van der Zande, A. Rigosi, H. M. Hill, S. H. Kim, J. Hone, Z. Li, D. Smirnov, and T. F. Heinz, Phys. Rev. Lett. **113**, 266804 (2014).

[40] J. Klein, A. H otger, M. Florian, A. Steinhoff, A. Delhomme, T. Taniguchi, K. Watanabe, F. Jahnke, A. Holleitner, M. Potemski, C. Faugeraus, J. Finley, and A. V. Stier, Phys. Rev. Research **3**, L022009 (2021).

[41] Z. Wang, K. F. Mak, and J. Shan, Phys. Rev. Lett. **120**, 066402 (2018).

[42] G. Plechinger, P. Nagler, A. Arora, A. Granados del Águila, M. Ballotin, T. Frank, P. Steinleitner, M. Gmitra, J. Fabian, P. Christianen, R. Bratschitsch, C. Schüller, and T. Korn, Nano Lett. **16**, 7899 (2016).

[43] T. Deilmann, P. Krüger, and M. Rohlfing, Phys. Rev. Lett. **124**, 226402 (2020).

[44] J. Förste, N. Tepliakov, S. Kruchinin, J. Lindau, V. Funk, M. Förg, K. Watanabe, T. Taniguchi, A. Baimuratov, and A. Högele, Nat. Commun. **11**, 4539 (2020).

[45] T. Woźniak, P. E. Faria, Jr., G. Seifert, A. Chaves, and J. Kunstmann, Phys. Rev. B **101**, 235408 (2020).

[46] C. Robert, H. Dery, L. Ren, D. Van Tuan, E. Courtade, M. Yang, B. Urbaszek, D. Lagarde, K. Watanabe, T. Taniguchi, T. Amand, and X. Marie, Phys. Rev. Lett. **126**, 067403 (2021).

[47] E. Liu, J. van Baren, Z. Lu, M. M. Altaiary, T. Taniguchi, K. Wtanabe, D. Smirnov, and C. H. Lui, Phys. Rev. Lett. **123**, 027401 (2019).

[48] M. Barbone, A. Montblanch, D. Kara, C. Palacios-Berraquero, A. Cadore, D. De Fazio, B. Pingault, E. Mostaani, H. Li, B. Chen, K. Watanabe, T. Taniguchi, S. Tongay, G. Wang, A. Ferrari, and M. Atature, Nat. Commun. **9**, 3721 (2018).

[49] See Supplemental Material at http://link.aps.org/supplemental/10.1103/PhysRevB.106.L081409 for additional information on the experimental setup, calibration measurements, supplemental measurements, and fitting, which includes Refs. [53–70].

[50] C. Jin, J. Kim, J. Suh, Z. Shi, B. Chen, X. Fan, M. Kam, K. Watanabe, T. Taniguchi, S. Tongay, A. Zettl, J. Wu, and F. Wang, Nat. Phys. **13**, 127 (2017).

[51] J. Jadczak, J. Kutrowska-Girzycka, J. Schindler, J. Debus, K. Watanabe, T. Taniguchi, C.-H. Ho, and L. Bryja, Materials **14**, 399 (2021).

[52] M. Rosenberger, H.-J. Chuang, K. McCreary, A. Hanbicki, S. Sivaram, and B. Jonker, ACS Appl. Mater. Interfaces **10**, 10379 (2018).

[53] A. Steinhoff, M. Florian, A. Singh, K. Tran, M. Kolarczik, S. Helmrich, A. W. Achstein, U. Woggon, N. Owschmikow, F. Jahnke, and X. Li, Nat. Phys. **14**, 1199 (2018).

[54] E. Liu, J. van Baren, C.-T. Liang, T. Taniguchi, K. Watanabe, N. M. Gabor, Y.-C. Chang, and C. H. Lui, Phys. Rev. Lett. **124**, 196802 (2020).

[55] M. Molas, C. Faugeras, A. Slobodeniuk, K. Nogajewski, M. Bartos, D. Basko, and M. Potemski, 2D Mater. **4**, 021003 (2017).

[56] X. Zhang, T. Cao, Z. Lu, Y.-C. Li, F. Zhang, Y. Wang, L. Zhiqiang, J. Hone, J. Robinson, D. Smirnov, S. Louie, and T. F. Heinz, Nat. Nanotechnol. **12**, 883 (2017).

[57] A. Kormányos, G. Nurkard, M. Gmitra, J. Fabian, V. Zólyomi, N. Drummond, and V. Fal'ko, 2D Mater. **2**, 022001 (2015).

[58] M. Manca, M. M. Glazov, C. Robert, F. Cadiz, T. Taniguchi, K. Watanabe, E. Courtade, T. Amand, P. Renucci, . Marie, G. Wang, and Urbaszek, Nat. Commun. **8**, 14927 (2017).

[59] T. O'Haver, *A Pragmatic Introduction to Signal Processing* (2021).

[60] P. K. Dasgupta, Y. Chen, C. Serrno, G. Guiochon, H. Liu, J. Fairchild, and R. Shalliker, Anal. Chem. **82**, 10143 (2010).

[61] M. Wahab, F. Gritti, T. O'Haver, G. Hellinghausen, and D. Armstrong, Chromatographia **82**, 211 (2019).

[62] O. Ajayi, J. Ardelean, G. Shepard, J. Wang, A. Antony, T. Taniguchi, K. Watanabe, T. F. Heinz, S. Strauf, X.-Y. Zhu, and J. Hone, 2D Mater. **4**, 031011 (2017).

[63] Y. Lin, X. Ling, L. Yu, S. Huang, A. Hsu, Y.-H. Lee, J. Kong, M. Dresselhaus, and T. Palacios, Nano Lett. **14**, 5569 (2014).

[64] X. Zhu, N. Monahan, Z. Gong, H. Zhu, K. Williams, and C. Nelson, J. Am. Chem. Soc. **137**, 8313 (2015).

[65] M. Newville, T. Stensitzki, D. B. Allen, and A. Ingargiola, LM-FIT: Non-linear least-square minimization and curve-fitting for Python (0.8.0) (Zenodo, 2014), https://doi.org/10.5281/zenodo.11813.

[66] K. Levenberg, Q. Appl. Math. **2**, 164 (1944).

[67] C. Chow, H. Yu, A. Jones, J. Yan, D. Mandrus, T. Taniguchi, K. Watanabe, W. Yao, and X. Xu, Nano Lett. **17**, 1194 (2017).

[68] J. Serrano, A. Bosak, R. Arenal, M. Krisch, K. Watanabe, T. Taniguchi, H. Kanda, A. Rubio, and L. Wirtz, Phys. Rev. Lett. **98**, 095503 (2007).

[69] Z. Jin, X. Li, J. T. Mullen, and K. W. Kim, Phys. Rev. B **90**, 045422 (2014).

[70] G. B. Liu, W. Y. Shan, Y. Yao, W. Yao, and D. Xiao, Phys. Rev. B **88**, 085433 (2013).

[71] C. Dean, A. Young, I. Meric, C. Lee, L. Wang, S. Sorgenfrei, K. Watanabe, T. Taniguchi, P. Kim, K. Shepard, and J. Hone, Nat. Nanotechnol. **5**, 722 (2010).

[72] E. Liu, J. van Baren, T. Taniguchi, K. Watanabe, Y.-C. Chang, and C. H. Lui, Phys. Rev. B **99**, 205420 (2019).

[73] Z. Li, T. Wang, Z. Lu, M. Khatoniar, Z. Lian, Y. Meng, M. Blei, T. Taniguchi, K. Watanabe, S. McGill, S. Tongay, V. Menon, D. Smirnov, and S.-F. Shi, Nano Lett. **19**, 6886 (2019).

[74] Z. Wang, L. Zhao, K. F. Mak, and J. Shan, Nano Lett. **17**, 740 (2017).

[75] H. Yu, G.-B. Liu, P. Gong, X. Xu, and W. Yao, Nat. Commun. **5**, 3876 (2014).

[76] A. Chernikov, A. M. van der Zande, H. M. Hill, A. F. Rigosi, A. Velauthapillai, J. Hone, and T. F. Heinz, Phys. Rev. Lett. **115**, 126802 (2015).

[77] J. Roch, N. Leisgang, G. Froelicher, P. Makk, K. Watanabe, T. Taniguchi, C. Schönenberger, and R. Warburton, Nano Lett. **18**, 1070 (2018).

[78] M. Koperski, M. Molas, A. Arora, K. Nogajewski, M. Bartos, J. Wyzula, D. Vaclavkova, P. Kossacki, and M. Potemski, 2D Mater. **6**, 015001 (2018).

[79] S. Das Sarma, E. H. Hwang, and Q. Li, Phys. Rev. B **80**, 121303(R) (2009).